Excitation into $5p^57p$ levels from the ground level and the $J=2$ metastable level of Xe

R. O. Jung, John B. Boffard, L. W. Anderson, and Chun C. Lin
Department of Physics, University of Wisconsin, Madison, Wisconsin 53706, USA
(Received 15 September 2009; published 7 December 2009)

We present experimental cross-section measurements for electron-impact excitation from the ground level and from the Xe($5p^56s$) $J=2$ metastable level into levels of the Xe($5p^57p$) manifold using the optical method. The magnitudes of cross sections for excitation out of the ground-state range from $(65-365)\times10^{-20}$ cm^2. Cross sections out of the ground level are also investigated for pressures ranging from 0.1–1.0 mTorr, and show moderate dependence (particularly at high energies) on pressure due to cascades from resonant levels. Cross sections for excitation out of the metastable level have peak magnitudes that are on average more than an order of magnitude larger than their ground-state counterparts. Furthermore, cross sections out of the metastable levels into the Xe($5p^57p$) levels as a function of energy display a surprising variety of shapes which are discussed in relation to oscillator strengths. Together, the ground state and metastable cross sections measured in this work are expected to be useful for optical diagnostics of plasmas containing xenon.

DOI: 10.1103/PhysRevA.80.062708 PACS number(s): 34.80.Dp, 52.20.Fs

I. INTRODUCTION

A. Motivation

The study of electron collisions with rare-gas atoms has been of constant interest over several decades due to its importance in advancing the understanding of fundamental atomic collision processes as well as for applications to many different gaseous discharges and plasmas. For the particular case of Xe discharges, two recent applications include mercury-free light sources [1], and space propulsion, i.e., xenon ion engines and Hall-effect thrusters (HETs) [2,3]. In the latter, xenon atoms are ionized in a discharge and the resulting ions are accelerated in order to generate thrust. Information about the operating conditions of the thruster can be extracted via an examination of the optical emissions from the discharge and plume regions of the engine. Proper treatment necessitates a collisional radiative model (CRM) accounting for all excitation and de-excitation mechanisms; however, often times there is insufficient experimental data which complicates the application of these models [2].

The magnitude and energy dependence of electron-impact excitation cross sections into different excited levels exhibit many regularities that can be understood in terms of a few fundamental properties connecting the initial and final levels. For example, prior measurements of the rare gases (Ne through Xe) have revealed that for excitation from the ground state into $np^5(n+1)p$ levels ($n=2$, 3, 4, 5 for Ne, Ar, Kr, Xe), the cross sections into levels with total angular momentum $J=0$ are typically some of the largest, whereas the cross sections into these same upper levels from the metastable levels are among the smallest [4]. Here, excitation into the $J=0$ $np^5(n+1)p$ levels from the $J=0$ and $J=2$ metastable levels is dipole-forbidden. Electron excitation cross sections which correspond to dipole-allowed processes tend to be much larger in magnitude and decrease less rapidly with increasing incident electron energy than cross sections corresponding to dipole-forbidden processes; with the magnitudes of the cross sections tending to scale with the corresponding optical oscillator strengths f_{ij} [4]. The heaviest rare gases Kr and Xe exhibit additional patterns not observed in Ne and Ar. Due to a larger spin-orbit interaction within the np^5 core, excited levels of Kr and Xe form distinct tiers associated with different values of the total np^5 core angular momentum j_c. For excitation from the ground state, cross sections are generally larger into the lower energy tier, as is also the case for excitation from the $J=2$ metastable level, which is located in the lower tier of the $np^5(n+1)s$ group [5,6]. In contrast, excitation cross sections out of the $J=0$ metastable level, which is located in the upper tier of the $np^5(n+1)s$ group, are largest for excitation into the upper tier $np^5(n+1)p$ levels [6].

Excluding the vacuum ultraviolet emissions from resonance levels, the emission spectrum of Xe is dominated by the $5p^56p\rightarrow5p^56s$ transitions in the 750–1100 nm wavelength range. We have previously measured cross sections into Xe($5p^56p$) levels from both the ground state [5] and from the $J=2$ metastable level [7]. Emissions from these levels have been used previously in plasma diagnostics; for instance in the trace rare gas optical emission spectroscopy (TRG-OES) technique for measuring the electron temperature of processing plasmas [8]. However, since the wavelengths of these emissions lie just beyond the visible range, Xe discharges typically have more of a blue hue, due in part, to Xe($5p^57p\rightarrow5p^56s$) emissions in the 460–503 nm wavelength range. This latter set of emissions is also useful for plasma diagnostics since this wavelength range coincides with prominent $Xe^+(5p^46p\rightarrow5p^46s)$ emission lines used in the diagnostics of Xe HETs [2]. Measurement of excitation cross sections into Xe($5p^57p$) levels from the ground state and metastable levels may thus be of great use in lighting and HET modeling. In addition, previous work on excitation out of the metastable levels of Ar have revealed interesting differences between cross sections into Ar($3p^54p$) [9] and Ar($3p^55p$) [10] levels, with a breakdown of the oscillator strength scaling in the latter. When combined with our earlier Xe($5p^56p$) metastable cross-section measurements [7], the Xe($5p^57p$) cross sections measured in this work provide a test of our understanding of fundamental collision processes.

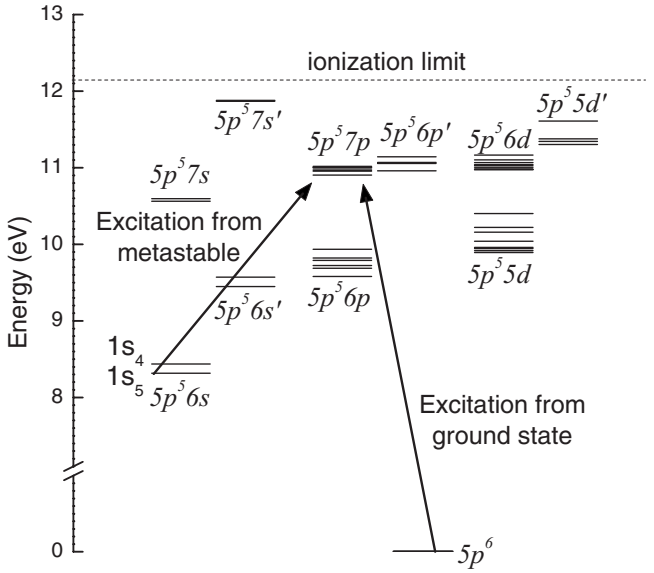

FIG. 1. Partial energy-level diagram for xenon. Levels associated with the $^2P_{1/2}$ ion core are indicated by a prime.

B. Atomic structure

The energy levels of interest in this work are illustrated in Fig. 1. The ground-state configuration of xenon is $1s^2 2s^2 2p^6 3s^2 3p^6 4s^2 3d^{10} 4p^6 5s^2 4d^{10} 5p^6$ which we abbreviate as $5p^6$. In the single configuration approximation, higher lying energy levels are obtained by promoting one of the outer $5p^6$ valence electrons into an excited orbital. For instance, by exciting a $5p$ electron into the $6s$ orbital we obtain the $5p^5 6s$ configuration which is comprised of four levels denoted $1s_2$ through $1s_5$ in Paschen's notation with J values of 1, 0, 1, and 2 respectively. The magnitude of the spin-orbit splitting between the $^2P_{3/2}$ and $^2P_{1/2}$ levels of the parent $5p^5$ ion core is much larger than any of the interaction terms of the outer $6s$ electron with the ion core. As a result, the energy levels of the $5p^5 6s$ are split into two tiers (separated by about 1.3 eV), with a lower grouping of $1s_5$ and $1s_4$ associated with the $^2P_{3/2}$ core, and an upper grouping of $1s_3$ and $1s_2$ associated with the $^2P_{1/2}$ core. For Xe the core angular momentum j_c is nearly a good quantum number for labeling the energy levels. When written in configuration notation, this upper group of levels, associated with the $^2P_{1/2}$ core ($j_c=1/2$), is indicated by a prime on the valence electron (e.g., $5p^5 6s'$). Of the four $5p^5 6s$ levels, the $1s_4$ and $1s_2$ ($J=1$ for both levels) are optically connected to the ground state ($J=0$) with radiative lifetimes on the order of nanoseconds. The $1s_5$($J=2$) and $1s_3$($J=0$) levels, however, are not optically connected to the ground state and are therefore metastable.

The $5p^5 7p$ configuration consists of six observed levels (labeled $3p_5$ through $3p_{10}$; $J=0,2,1,3,2,1$ in order of descending energy), associated with the $^2P_{3/2}$ core ($j_c=3/2$). The four levels of the $5p^5 7p$ configuration associated with the $^2P_{1/2}$ core ($3p_1$ through $3p_4$, $J=1,2,1,0$) have energies that lie above the ionization limit and are not experimentally observed. Table I lists wavelengths [11] and branching fractions [12] for the Xe($5p^5 6s - 5p^5 7p$) transition array. In addition to Paschen's notation, the excited levels of Xe are also widely labeled using Racah notation for which a $5p^5 nl$ level is labeled by $nl[K]_J$, where K is the intermediate vector sum of j_c and l. Both labeling schemes are included in Table I.

C. Optical method

All cross sections reported in this work are measured via the optical method, which has been described in detail elsewhere [13]. Therefore we only provide a brief description of the basic nomenclature. In the optical method, the cross section for excitation into an excited level j can be related to the photon flux out of that same level. Experimentally, a monoenergetic electron beam of current per unit area I is passed through and excites target atoms into various excited levels. Excited level j may be populated either by direct excitation from an initial level i (in this work, i is either the ground level or the $1s_5$ metastable level), or from radiative decay of higher lying levels k into j. Level j can then decay, giving off a photon, into any one of a number of lower levels α. Expressed as a rate equation, the population of level j, n_j, can be written as

$$\frac{dn_j}{dt} = \left(\frac{I}{e}\right) n(i) Q_j^{\mathrm{dir}} + \sum_{k>j} n_k A_{kj} - \sum_{\alpha<j} n_j A_{j\alpha}. \qquad (1)$$

The first term on the right accounts for the increase in n_j from the direct excitation from level i having density $n(i)$.

TABLE I. Wavelengths [11] and branching fractions [12] for the Xe($5p^5 6s - 5p^5 7p$) transition array. Dipole-forbidden transitions are left blank. Note that the branching fractions out of a given $3p_y$ upper level when summed over the four $1s_x$ levels do not equal one due to the additional decay channels to $5p^5 7s$ and $5p^5 5d$ levels.

Racah	Paschen	$7p[\frac{1}{2}]_0$ $3p_5(J=0)$	$7p[\frac{3}{2}]_2$ $3p_6(J=2)$	$7p[\frac{3}{2}]_1$ $3p_7(J=1)$	$7p[\frac{5}{2}]_3$ $3p_8(J=3)$	$7p[\frac{5}{2}]_2$ $3p_9(J=2)$	$7p[\frac{1}{2}]_1$ $3p_{10}(J=1)$
$6s'[\frac{1}{2}]_1^o$	$1s_2(J=1)$	857.60 nm 0.36	869.22 nm 0.12	864.85 nm 0.24		895.28 nm 0.09	930.66 nm 0.45
$6s'[\frac{1}{2}]_0^o$	$1s_3(J=0)$			796.73 nm 0.34			852.26 nm 0.04
$6s[\frac{3}{2}]_1^o$	$1s_4(J=1)$	480.70 nm 0.30	484.33 nm 0.07	482.97 nm 0.06		492.32 nm 0.13	502.83 nm 0.02
$6s[\frac{3}{2}]_2^o$	$1s_5(J=2)$		462.43 nm 0.26	461.19 nm 0.003	467.12 nm 0.31	469.70 nm 0.10	479.26 nm 0.01

The quantity (I/e) represents the electron flux per unit area of the electron beam passing through the target (e is the elementary charge). Q_j^{dir} is the *direct* cross section for excitation from i to j. The second term accounts for the increase in n_j due to *cascades* from higher levels k and contains a sum over all possible levels (having densities n_k) that may radiatively decay into level j. A_{kj} is the transition probability for radiative decay from level k to j. The third term accounts for the losses from level j by radiative decay to levels α with transition probabilities $A_{j\alpha}$.

In steady state, Eq. (1) simplifies into

$$Q_j^{\mathrm{dir}} = \sum_{j>\alpha} \frac{n_j A_{j\alpha}}{(I/e)n(i)} - \sum_{k>j} \frac{n_k A_{kj}}{(I/e)n(i)}, \tag{2}$$

with *optical emission* cross sections further defined as

$$Q_{j\to\alpha}^{\mathrm{opt}} = \frac{n_j A_{j\alpha}}{(I/e)n(i)}, \tag{3}$$

$$Q_{k\to j}^{\mathrm{opt}} = \frac{n_k A_{kj}}{(I/e)n(i)}, \tag{4}$$

so that Eq. (2) can be re-written as

$$Q_j^{\mathrm{dir}} = \underbrace{\sum_{j>\alpha} Q_{j\to\alpha}^{\mathrm{opt}}}_{Q_j^{\mathrm{app}}} - \underbrace{\sum_{k>j} Q_{k\to j}^{\mathrm{opt}}}_{Q_j^{\mathrm{cas}}}. \tag{5}$$

The first summation on the right-hand side is often referred to as the *apparent* cross section, Q_j^{app}, while the second summation is referred to as the *cascade* cross section, Q_j^{cas}.

Thus, in order to measure the direct cross section for excitation into j, one must measure all of the optical emission cross sections out of j (to obtain the apparent cross section) as well as measure all of the optical emission cross sections into j (to obtain the cascade cross section) as per Eq. (5). The measurement of the large number of required optical emission cross sections is complicated by the wide range of wavelengths (uv to ir) spanned by the emissions. For the apparent cross sections, however, this task can be simplified if the branching fractions, $\Gamma_{j\to\alpha}$, out of level j are known. Since the optical emission cross section can be written as

$$Q_{j\to\alpha}^{\mathrm{opt}} = \Gamma_{j\to\alpha} Q_j^{\mathrm{app}}, \tag{6}$$

by measuring a single optical emission cross section out of level j (having wavelength $\lambda_{j\to\alpha}$), and dividing by the appropriate branching fraction listed in Table I, the apparent cross section can be obtained.

II. EXCITATION FROM THE GROUND STATE

A. Experimental method

Optical emission cross sections for electron-impact excitation into levels of the Xe($5p^57p$) configuration out of the ground state were measured in the 450–900 nm wavelength range using an experimental apparatus described previously [13,14]. Briefly, a variable-energy, monoenergetic, electron beam is generated using a six element electron gun with an indirectly heated barium oxide cathode. The electron-beam current is collected by a deep Faraday cup and recorded by a computer. The electron gun is located in a vacuum chamber that is evacuated to 10^{-8} Torr and then backfilled with a static gas target using 99.995% purity Xe. Measurements were made for pressures in the range of 0.1 to 2.0 mTorr as measured by a spinning rotor gauge. Fluorescence from the decay of excited atoms exits the collision region through a narrow slit in the side of the Faraday cup and is imaged onto the entrance slits of a 1.26 m Czerny-Turner monochromator using a spherical mirror with unit magnification. Normal resolution was 0.15 nm full width at half maximum (FWHM), with higher resolutions employed in cases of contamination by other neutral or ion lines.

The light was ultimately detected by a thermoelectrically cooled RCA 31034A-02 GaAs photomultiplier tube (PMT) operating in photon counting mode. At each fixed step of the electron-beam energy, separate counts are recorded with the electron beam on and off as the beam is chopped at 250 Hz. Radiometric calibration of the detection system at each of the 16 separately measured transitions was performed by using a NIST-traceable calibrated quartz-tungsten-halogen lamp. In addition to the Xe($5p^57p\to5p^56s$) emission lines required for this work, additional optical emission cross-section measurements were performed to verify the absolute calibration by comparing with previous He [15] and Xe [5] cross-section results.

In general, optical emission cross sections must be corrected for any polarization of the emitted radiation. Emissions from the collision region are only collected from a direction perpendicular to the electron-beam axis, hence if the emission pattern of the fluorescence is not isotropic, a correction to the measured intensity must be included to obtain accurate cross-section results [13]. This correction amounts to a factor of $(1-P/3)$ where P is the polarization of the emitted radiation. Measurements of the polarization of emissions from Xe($5p^57p$) levels taken at a variety of electron energies were generally less than ±0.06, with a maximum magnitude of -0.14. Due to the small size of the resulting correction factor to the cross-section values ($\leq5\%$), the effects of polarization have been neglected in the values reported here.

B. Results of apparent excitation cross sections and pressure dependence

Values of the optical emission cross sections for the Xe($5p^57p\to5p^56s$) transition array at an electron energy of 19 eV are presented in Table II (see Table I for corresponding wavelengths). The total uncertainty in these measurements is approximately $\pm15\%$ with the two largest sources being the radiometric calibration and the statistical uncertainties (particularly for the weakest emission lines). In addition to the measured emissions into the Xe($5p^56s$) levels, Xe($5p^57p$) atoms also have substantial emissions into levels of the Xe($5p^57s$) and Xe($5p^55d$) configurations with wavelengths in the 1.1–4.0 μm range. In our previous measurements of cross sections for the Xe($5p^56p$) levels, additional optical emission cross sections in the 900–2800 nm wavelength

TABLE II. Optical emission cross sections for excitation out of the ground state at 19 eV measured at 1.0 mTorr. Entries for dipole-forbidden transitions are left blank. Values obtained via branching fractions are indicated in parenthesis. Uncertainties in total apparent cross sections, Q^{App}, include statistical and systematic uncertainties from measured emission cross sections and the additional uncertainties introduced by using branching fractions from Ref. [12] to fill in unmeasured transitions. Uncertainty in the measured optical emission cross sections are approximately ±15%.

	Cross Section (10^{-20} cm^2)					
Lower level	$3p_5(J=0)$	$3p_6(J=2)$	$3p_7(J=1)$	$3p_8(J=3)$	$3p_9(J=2)$	$3p_{10}(J=1)$
$1s_2(J=1)$	24	29	89		17[a]	(88)
$1s_3(J=0)$			124			7.0
$1s_4(J=1)$	20	17	24		23	3.5
$1s_5(J=2)$		60	1.1	72	17	2.3
$\Sigma 5p^5 7s$	(13)	(84)	(61)	(108)	(61)	(29)
$\Sigma 5p^5 5d$	(9.5)	(47)	(65)	(53)	(66)	(64)
Q^{App}	(66.5 ± 11)	(237 ± 40)	(364 ± 60)	(233 ± 44)	(184 ± 35)	(193.8 ± 39)

[a] ±25% uncertainty due to difficulty in resolving this line (895.28 nm) from the much stronger 895.23 nm line.

range were measured using a Fourier transform spectrometer (FTS) [5]. Unfortunately, almost all of the optical emission cross sections into and out of the Xe($5p^5 7p$) levels in this wavelength range are too small to reliably measure owing to the relatively poor sensitivity of ir detectors. Instead, the Xe($5p^5 7p \rightarrow 5p^5 7s$) and Xe($5p^5 7p \rightarrow 5p^5 5d$) optical emission cross sections were obtained by combining the measured Xe($5p^5 7p \rightarrow 5p^5 6s$) optical emission cross sections with branching fraction measurements made with a bright Xe hollow cathode lamp [12]. With these values, it is possible to obtain apparent cross sections into the Xe($5p^5 7p$) levels by summing all the optical emission cross sections out of each Xe($5p^5 7p$) level. The uncertainties in these values, included in the last row of Table II, are larger than those of the optical emission cross sections due to the added uncertainties in the branching fractions. The energy dependence of the apparent cross sections are illustrated in Fig. 2.

In addition to direct electron-impact excitation from the ground state, Xe($5p^5 7p$) levels can also be populated by excitation into higher levels that radiatively cascade down to the Xe($5p^5 7p$) levels. In principle, the direct excitation cross section into each level can be obtained from the apparent cross section by subtracting off the sum of all optical emission cross sections terminating on Xe($5p^5 7p$) levels [see Eq. (5)]. In practice, however, this is exceedingly difficult since most of these cascade transitions are again in the mid to far infrared for the Xe($5p^5 7p$) levels where reliable measurements are, again, difficult in this wavelength range. Hence, only apparent cross sections are reported in this work.

Among the levels that cascade into $5p^5 7p$ levels are $J=1$ levels of the $5p^5 ns$ and $5p^5 nd$ configurations. In addition to decaying into levels of the $5p^5 7p$ configuration, these resonance levels can also radiatively decay to the $J=0$ $5p^6$ ground state. Radiation trapping of these resonance transitions due to the presence of ground-state Xe atoms leads to a pressure dependence in the $5p^5 ns, 5p^5 nd \rightarrow 5p^5 7p$ emissions [5]. As the pressure in the chamber is increased, the resonance transition is more likely to be reabsorbed before leaving the vacuum chamber. As a result, the effective branching fraction to the ground state is decreased, while the branching fractions to the $5p^5 7p$ levels, which are not reabsorbed, increase with a rise in ground-state density/pressure. Due to the

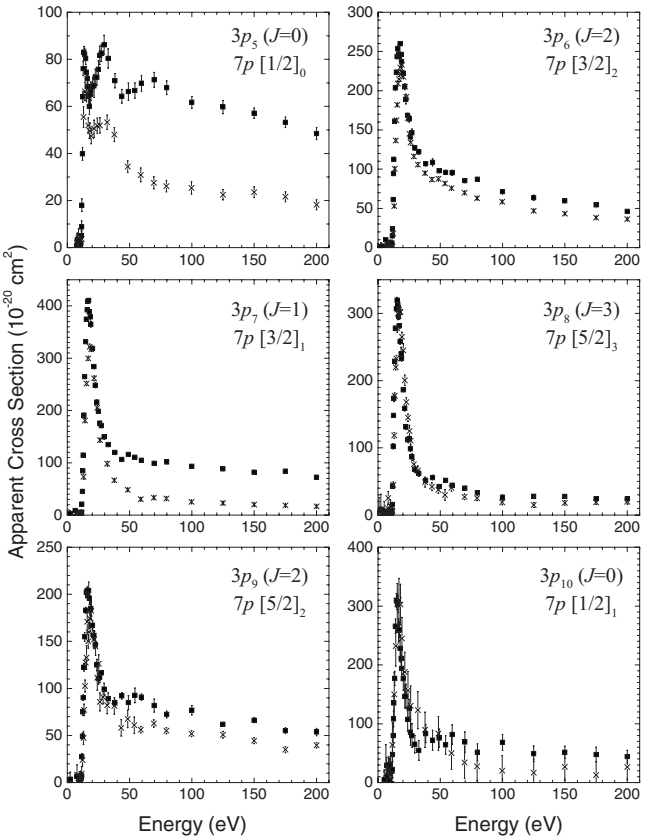

FIG. 2. Apparent excitation cross sections out of the ground state into Xe($5p^5 7p$) levels. Cross sections were measured at both 1 mTorr (■), and 0.1 mTorr (×). Error bars are statistical only and do not include the uncertainties in the absolute calibration (~15%) and transition probabilities used to convert Q^{Opt} to Q^{App}.

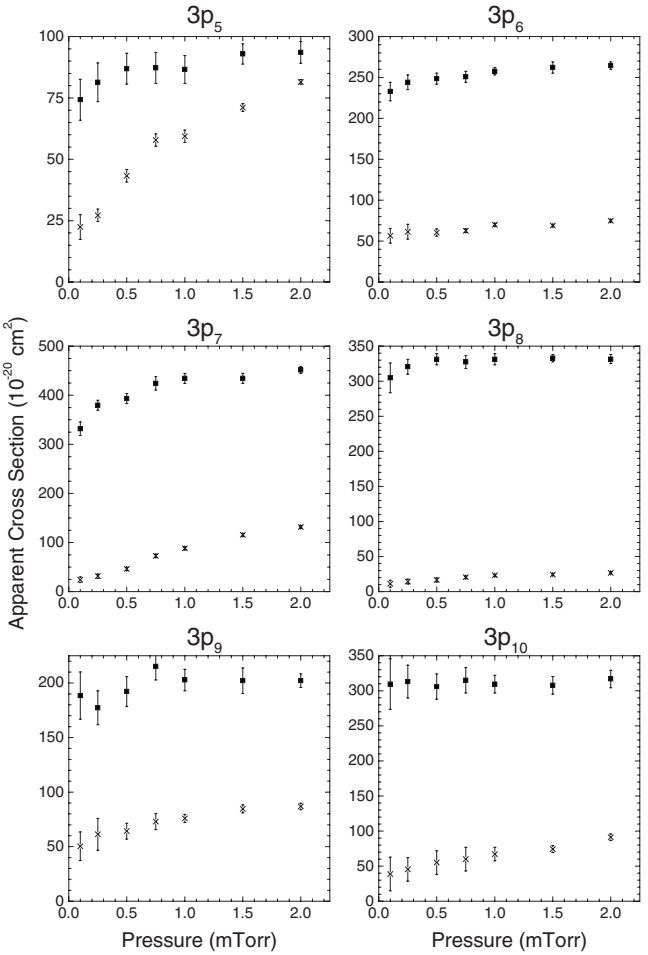

FIG. 3. Pressure dependence of the measured Xe($5p^57p$) cross sections at two energies, peak (■, nominally 14–16 eV), and at 100 eV(×). Error bars are statistical only.

pressure dependent cascades, the measured Xe($5p^57p$) apparent and optical emission cross sections exhibit some degree of pressure dependence as illustrated in Fig. 3. In principle, by measuring and then subtracting off this cascade contribution to the apparent cross section, it is possible to show that the direct excitation cross section is independent of pressure as was done in our earlier work on cross sections for excitation into Xe($5p^56p$) levels where the major cascade contributions could be measured more easily [5].

For dipole-allowed excitation processes, such as excitation from the ground state into the $J=1$ resonance levels of the $5p^5ns$ and $5p^5nd$ configuration, the shape of the excitation function is that of a broad curve (E^{-1} ln E energy dependence) with a peak located at an energy of a few times the threshold energy. In comparison, the direct excitation cross sections into the $5p^57p$ levels from the ground state are expected to peak very close to threshold with a E^{-1} or E^{-3} energy dependence at high energies. Thus, at low energies (i.e., at the peak) where the direct excitation into the $5p^57p$ dominates, the measured Xe($5p^57p$) cross sections generally display little pressure dependence as illustrated by the solid square data in Fig. 3. In contrast, at an electron energy of 100 eV the direct cross section into the various Xe($5p^57p$) levels are generally small whereas cross sections into cascading resonance levels are near their peak values, leading to a much larger pressure dependence. This is also evident in the shape of the apparent cross sections measured at 0.1 and 1.0 mTorr plotted in Fig. 2. At low energies, the two curves are almost identical, whereas the 1.0 mTorr curves for most levels are larger at higher energies (>50 eV).

C. Discussion

The shapes of the 1.0 mTorr ground-state excitation functions in Fig. 2 vary from sharp peaks for the $3p_8$ and $3p_{10}$ levels to intermediate width peaks for the $3p_6$, $3p_7$, and $3p_9$ levels, leaving the $3p_5$ level in a class by its own with three distinct peaks at 13, 30, and 70 eV. By comparing these shapes with those measured at 0.1 mTorr where the cascade contribution from resonance levels are greatly reduced, it is clear that cascades contribute substantially to the high-energy shapes of the $3p_5$ and $3p_7$ levels. Indeed, the third high-energy peak in the $3p_5$ excitation function completely disappears when measured at 0.1 mTorr and the $3p_7$ shape changes to that of a sharp peak. It is interesting to note that while the 0.1 mTorr apparent excitation functions for both the $3p_6$ and $3p_9$ levels are somewhat reduced at high energies, they both still have a significant high-energy tail.

The shape of these Xe($5p^57p$) excitation functions is similar to what was observed for the Xe($5p^56p$) levels [5]. Both the apparent and direct excitation cross sections for the $J=3$ $2p_8$ and $J=1$ $2p_{10}$ levels were sharply peaked. The $J=2$ $2p_6$ and $2p_9$ levels had intermediate width peaks in their apparent cross sections that did not completely disappear upon subtracting off the full cascade contribution. The shape of the $J=1$ $2p_7$ excitation function changed from a wide peak (apparent cross section) to an intermediate width peak (direct cross section) upon subtraction of the cascades. The shape of the apparent and direct excitation functions are both relatively broad for the $J=0$ $2p_5$ level. The shape of the $2p_5$ apparent excitation function in Ref. [5] includes only a single peak at 30 eV compared to the three peaks observed for the $3p_5$ level; however, the direct cross section for the $2p_5$ level does exhibit a small shoulder at 14 eV in addition to the main peak at 30 eV. Measurements of the $2p_5$, $3p_5$, $4p_5$, $5p_5$, and $7p_5$ excitation functions made at 2.2 mTorr reveal that only the $3p_5$ level has a distinct low-energy (~13 eV) peak, with the other excitation functions having only a shoulder at this energy [16]. In a study of excitation into the Xe np_5 levels ($n=2$ to 9), Smirnov also noted that the $3p_5$ level stands apart from the cross sections into the other np_5 levels in both the shape of the excitation function and magnitude of the cross section [17].

The differences in the shape of the excitation functions for the three levels with narrow excitation functions at low pressure ($3p_7$, $3p_8$, and $3p_{10}$) and the three with broad excitation functions ($3p_5$, $3p_6$, and $3p_9$) can be understood in terms of a multipole field analysis [4]. For an intuitive exposition of this analysis, we think of the excitation process as an absorptionlike transition caused by the electromagnetic field associated with the colliding electron which can be decomposed into monopole ($k=0$), dipole ($k=1$), quadrupole ($k=2$),… components. For excitation from the $5p^6$ ground state to

$5p^57p$ levels, the active electron jumps from an $l=1$ orbital to another $l=1$ orbital. Only the $k=0$ and $k=2$ components are compatible with the $l=1\rightarrow l=1$ transition of the active electron. With respect to the quantum number J, the $k=0$ component connects the ground state $5p^6(J=0)$ directly only to the $J=0$ levels of the $5p^57p$ configuration whereas the $k=2$ component connects the ground state only to the $J=2$ levels of $5p^57p$. Thus the $J=0$ and $J=2$ levels are favored as the final state. Excitation into the $J=1$ and $J=3$ must proceed via interactions of higher order and hence are expected to have smaller cross sections. Indeed, the apparent cross sections at 100 eV into the three levels with even J, $3p_5(J=0)$, $3p_6(J=2)$, and $3p_9(J=2)$, are on average a factor of two larger than the cross sections into the three levels with odd J, $3p_7(J=1)$, $3p_8(J=3)$, and $3p_{10}(J=1)$. A full account of the theoretical foundation of the multipole field model may be found in Ref. [4].

D. Comparison with previous measurements

Values for some of the Xe($5p^57p\rightarrow 5p^56s$) optical emission cross sections have been previously reported in Refs. [2,17–19]. Chiu *et al.* recently measured electron-impact optical emission cross sections for 12 Xe and Xe^+ lines in the 450–550 nm range [2]. The measurements, made at a pressure of 1.5 mTorr, are reported for electron energies from 10 to 70 eV in 5 eV steps. Due to contamination of some lines by ion line emissions (26 eV threshold for excitation from the atomic ground state), we compare only peak cross section values. For the 480.7 nm ($3p_5$), 484.3 nm ($3p_6$), and 492.3 nm ($3p_9$) emission lines the peak cross sections of Chiu *et al.* [2] are within $\pm 10\%$ of the values reported here. For the 467.1 nm ($3p_8$) line the peak value of Ref. [2] is 23% smaller than the value measured in this work; however, this difference may be due to the sharp peak of the $3p_8$ excitation function falling between the 5 eV steps listed in Ref. [2]. While our two experiments are in good agreement for the 484.3 nm optical emission cross section, the values for the 462.4 nm line arising from the same $3p_6$ upper level differ by 30%. The branching ratio for these two $3p_6$ lines extracted from the cross section values reported in Ref. [2] is incompatible with the values reported here and in other sources [12,20,21].

While the 0.1 mTorr $3p_5$ excitation function measured in this work is in reasonable agreement with the shape measured at the same pressure by Smirnov [17], the magnitudes of the $3p_5\rightarrow 1s_2$ (857.6 nm) and $3p_5\rightarrow 1s_4$ (480.7 nm) optical emission cross sections measured by Smirnov differ substantially from the values reported here. Large variations in effective branching fractions also make it difficult to compare the present results with the early results of Refs. [18,19]. For example, the average difference between peak cross-section values measured in this work and those of Ref. [18] is less than $\pm 17\%$ for six emission lines, but greater than $\pm 50\%$ for four other lines. The branching fractions, extracted from the optical emission cross sections in Ref. [18], for each of the lines with poor agreement differ dramatically from the branching fractions measured in this work which are compatible with a number of other experimental measurements [12,20,21].

E. Comparison with excitation into Xe($5p^56p$)

Our previous experiments on electron excitation from the ground state into the ten Xe($5p^56p$) levels revealed a striking feature not seen in the lighter rare gases [4]. This refers to the drastically larger cross sections observed for the lower six levels with $j_c=3/2$ than the upper four levels with $j_c=1/2$. For instance at 30 eV, the average direct excitation cross sections for the lower six levels and for the four upper levels are 628×10^{-20} and 173×10^{-20} cm^2, respectively [5]. This was explained on the grounds that because of the large spin-orbit coupling of the $Xe^+(5p^5)$ core, the two groups of levels are separated by 1.3 eV with ionization energies of 2.4 eV ($j_c=3/2$ group) and 1.1 eV ($j_c=1/2$ group). For hydrogen atoms the orbital radius (expectation value of r) is inversely proportional to the ionization energy. This inverse relation is well recognized for many-electron atoms and utilized in the approximate method of Bates and Damgaard [22] in which the exponential width of the wave function is obtained from the observed ionization energy. Thus the $5p^56p$ levels in the upper group have more spatially extended electron densities than those in the lower group and therefore smaller cross sections for excitation from the ground state which has a very compact wave function.

In the present work, we study excitation into only the lower group of Xe($5p^57p$) because the upper four levels ($j_c=1/2$) of this configuration lie above the $Xe^+(5p^5\ ^2P_{3/2})$ ionization limit. Interestingly as shown in Fig. 1 the Xe($5p^57p$) levels reported here and the upper group of Xe($5p^56p$) levels, labeled $5p^56p'$, have nearly the same ionization energy, thus their wave functions are expected to have comparable range. The average excitation cross section of the six levels of Xe($5p^57p, j_c=3/2$) at 30 eV is 94×10^{-20} cm^2 as compared to an average of 173×10^{-20} cm^2 for the four levels of Xe($5p^56p, j_c=1/2$). The smaller cross sections for Xe($5p^57p, j_c=3/2$) levels are to be expected since excitation into a level of higher principal quantum number is generally less favorable.

III. EXCITATION FROM THE $1s_5$ LEVEL

A. Experimental method

The apparatus for measuring cross sections for excitation out of the metastable level used in our laboratory is very different from the one used for excitation from the ground level because the metastable atom targets are generated in the form of an atomic beam emerging from a discharge whereas ground-state excitation experiments entail only a static gas. Experimental details for excitation of metastable atoms have been described in more detail in our previous work on argon [9] and xenon [7], therefore only a short description is given here. Metastable Xe atoms are created in a hollow cathode discharge supplied with a mixture of 85% He and 15% Xe at a total pressure of 4.5 Torr. The added helium reduces sputtering of the cathode and stabilizes the discharge so a substantial population of metastable Xe atoms is created. A small (1 mm diameter) hole in the base of the cathode allows atoms to exit into the collision region where they are crossed by a monoenergetic electron beam. A 1000

l/s diffusion pump maintains a background pressure of 3×10^{-4} Torr as measured near this collision region. Electrons in the beam excite the metastable atoms into various levels within the $5p^5 7p$ manifold. For each fixed value of the electron-beam energy, fluorescence from the decay of a particular excited level is isolated by a narrowband interference filter (0.3–1.0 nm FWHM) and detected by a PMT operating in photon counting mode. For this work, the observed wavelengths lie in the range of 462.4–502.8 nm, all of which are detectable by an EMI 9658B (S-20 cathode) PMT. The optical detection axis lies at 60° from the electron beam, which is close to the "magic angle" of 54.7° where the emission intensity is equal to the isotropic value for all polarizations [13]. Since the detection system consisting of the PMT and interference filter is polarization insensitive, no polarization correction to the cross sections is required.

The atomic beam exiting the cathode contains (i) atoms in the ground state, (ii) atoms in long-lived Xe($5p^5 6s$) levels, and (iii) atoms in a variety of short-lived excited levels. Atoms in these short-lived levels decay to the ground state before reaching the collision region leaving only atoms of categories (i) and (ii). The exact composition of $5p^5 6s$ levels in the collision region was measured via laser induced fluorescence (LIF). For these LIF measurements, a single mode Ti:Sapphire laser pumped by an 8 W argon ion laser is employed. We find the ratio of $1s_5:1s_3$ metastable atoms to be in excess of 200:1 for our particular operating conditions. Thus, the signal arising from excitation of $1s_3$ atoms contributes insignificantly to the total signal for all metastable cross sections measured in this work. Furthermore, LIF measurements also confirm the absence of atoms in the short-lived $1s_2$ and $1s_4$ resonance levels within the collision region.

For electron energies below the threshold for ground-state excitation (~11 eV), the signal collected is due entirely to excitation out of the $1s_5$ metastable level. However, since most of the atoms exiting the discharge are in the ground state ($n_g/n_m \approx 10^5$), for electron energies above the threshold for ground-state excitation, the signal arising from excitation of the large number of ground-state atoms in the target completely overwhelms the smaller metastable contribution. Therefore, reliable data can only be obtained for electron energies $\lesssim$10 eV.

B. Absolute calibration

The method used to place the results on an absolute scale is the same method we have used to calibrate previous cross-section measurements [10]. The optical emission signal S_i for a particular wavelength λ measured as a function of energy E can be expressed as

$$S_i(E) = C\xi_\lambda n(i) Q_i(E) I_e(E), \tag{7}$$

where Q_i is the excitation cross section out of level i, $n(i)$ is the number density of atoms in level i, $I_e(E)$ is the electron-beam current at energy E, and ξ_λ is the optical efficiency of the detection system at a wavelength λ. The constant C encompasses various conversion factors, the solid angle of the detection optics, as well as the overlap integrals of the electron beam and atomic beam in the viewing region.

Accurate determination of the quantities $\xi_\lambda, n(i)$, and especially C is experimentally difficult so we instead employ a ratio technique to eliminate these quantities and extract the cross section $Q_i(E)$. This technique involves comparing the emissions from the desired $3p_x$ level to the emissions from the $2p_6$ level for which the ground state and metastable cross sections have been previously measured [5,7]. Four separate signals are required to form the ratio: (a) the emission signal representing metastable excitation into the desired $3p_x$ level $S_m^{3p_x}$; (b) the emission signal for ground-state excitation at the same wavelength $S_g^{3p_x}$; (c) the emission signal representing metastable excitation into the $2p_6$ level $S_m^{2p_6}$ (at 823.1 nm); and (d) the emission signal for ground-state excitation $S_g^{2p_6}$ (also at 823.1 nm). The ratio of signal rates (a) and (b) removes the dependence on C and ξ_λ, however leaving behind a ratio of the metastable to ground-state number densities (n_m/n_g). This quantity, being difficult to measure, is removed by dividing the ratio of (a) to (b) by the ratio of (c) to (d), canceling out the number density ratio. Denoting the optical emission cross section for a spectral line originating from the np_x level at a wavelength of λ due to excitation out of the ground state as $Q_{np_x;\lambda}^{\mathrm{opt}(g)}$ and the corresponding cross section due to excitation out of the metastable level as $Q_{np_x;\lambda}^{\mathrm{opt}(m)}$, we have

$$Q_{3p_x;\lambda}^{\mathrm{opt}(m)}(E) = \frac{S_m^{3p_x}(E)}{S_m^{2p_6}(E)} \frac{S_g^{2p_6}(E')}{S_g^{3p_x}(E')} \frac{Q_{3p_x;\lambda}^{\mathrm{opt}(g)}(E')}{Q_{2p_6;\lambda'}^{\mathrm{opt}(g)}(E')} Q_{2p_6;\lambda'}^{\mathrm{opt}(m)}(E). \tag{8}$$

Here, E is the energy (8 eV) at which the metastable measurements are calibrated while E' is the energy (16 eV) used for the ground-state measurements. We use the optical emission cross section for excitation from the ground state into the $2p_6$ level of Ref. [5]. Cross sections into the $3p_x$ levels from the ground state are taken from Sec. II B. The cross section for excitation from the $1s_5$ metastable level into the $2p_6$ level is taken from our previous work [7].

Optical emission cross sections calibrated using Eq. (8) are equal to the total *apparent* cross section times the branching fraction for the observed $3p_x \rightarrow 1s_y$ emission line. Thus to obtain apparent cross sections, one need only measure the optical emission cross section for a single decay channel and divide by the known branching fraction for that emission line [see Eq. (6)]. In this manner, we are able to provide apparent cross-section values for excitation out of the $1s_5(J=2)$ metastable level into levels of the $5p^5 7p$ manifold.

C. Cascade estimates

In the preceding sections we discuss measurements of apparent excitation cross sections. To obtain the direct excitation cross sections, one must determine the optical emission cross sections for the cascading transitions as illustrated in Eq. (5). For excitation out of the *ground state* into the Ne($2p^5 3p$), Ar($3p^5 4p$), Kr($4p^5 5p$), and Xe($5p^5 6p$) levels reported in Refs. [5,23–25], the cascade cross sections were actually measured experimentally to evaluate the direct excitation cross sections. Although similar measurements, in principle, can be performed for excitation out of the metastable levels into the same set of $np^5(n+1)p$ levels, the sig-

TABLE III. Apparent cross sections for excitation from the $1s_5$ metastable level at selected incident electron energies. Uncertainties in the values are ±40%.

Energy (eV)	Apparent cross section (10^{-16} cm^2)				
	$3p_5$	$3p_6$	$3p_7$	$3p_8$	$3p_9$
3	0.008	0.12	0.076	0.41	0.25
4	0.156	0.43	0.464	1.18	0.43
5	0.129	0.35	0.251	1.10	0.34
6	0.089	0.36	0.201	1.24	0.28
7	0.054	0.37	0.243	1.17	0.30
8	0.053	0.35	0.144	1.10	0.32
9	0.076	0.34	0.068	1.17	0.34

nal levels for the cascading emissions were too small to detect. As to excitation into the higher members $np^5(n+2)p$, the cascade emissions are in the far-infrared precluding direct measurements even in the case of ground-state excitation.

In lieu of direct measurements we have devised a model for estimating cascades for the case of excitation out of the metastable levels. Details of this model are discussed in the Appendix. We have applied this model to address the cascades in connection with excitation into the Ar($3p^54p$), Ar($3p^55p$), Xe($5p^56p$), and Xe($5p^57p$) levels from the metastable levels. For the case of Ar($3p^54p$), our model gives the cascade component as 17% of the apparent excitation cross section, in reasonable agreement with the estimate of 10% based on the time-resolution-like experiment of Ref. [9]. We obtain a significantly larger cascade component of 27% for Ar($3p^55p$) which is also consistent with the estimates given in Ref. [10]. The Xe($5p^56p$) is found to have 21% cascade in line with its lighter analog Ar($3p^54p$). Our special interest in this paper is, of course, Xe($5p^57p$) and here we have a rather unusual situation. Of the levels capable of cascading into Xe($5p^57p$), the Xe($5p^56d$) group is most favorably populated by excitation out of the metastable level. However, the $5p^56d \rightarrow 5p^57p$ emissions have negligibly small transition probabilities due to the extraordinarily small frequencies (equivalent to ΔE_{ij} of 0.07 eV) eliminating what normally would be the major source of cascade. As a result we estimate the cascade to be less than 10%. See Appendix for details of this calculation. With such a small cascade component, the apparent excitation cross sections of Xe($5p^57p$) reported in this work can be taken as direct excitation cross sections to a good approximation.

D. Results and discussion

Apparent cross sections for excitation from the metastable level into the $3p_5$ through $3p_9$ levels measured as a function of incident electron energy are listed in Table III and plotted in Fig. 4. Error bars shown represent the statistical uncertainty only and do not reflect the systematic uncertainty (~40%) associated with placing the results on an absolute scale. Table IV lists optical emission cross sections at 8 eV obtained from combining the apparent cross-section values in Table III and branching fractions from Ref. [12] in accordance with Eq. (6).

We do not report a cross section for excitation into the $3p_{10}$ level since all of the possible emission lines were (i) too weak to provide a measurable signal, (ii) outside the favorable detection range of the PMT, or (iii) contaminated by other nearby emission lines arising from the excitation of helium or xenon. This latter case is only a problem on the hollow cathode system as the interference filters used for spectral isolation have a FWHM of 0.3–1.0 nm, while the monochromator system used in the ground-state apparatus can attain a much higher resolution (i.e., <0.15 nm FWHM; see Sec. II A).

The excitation cross sections reported in this paper fall into two classes: dipole-allowed ($1s_5 \rightarrow 3p_8$, $3p_6$, $3p_9$, $3p_7$ corresponding to $J=2 \rightarrow J=3,2,2,1$) and dipole-forbidden ($1s_5 \rightarrow 3p_5$ corresponding to $J=2 \rightarrow J=0$). Discussion of dipole-allowed excitation is facilitated by the Born-Bethe theory where the cross section for $i \rightarrow j$ excitation $Q_{ij}(E)$ as a function of energy is expanded as a leading $E^{-1} \ln E$ term followed by higher-order members in the powers of E^{-n},

$$Q_{ij}^{BB}(E) \simeq 4\pi a_o^2 f_{ij} \frac{R^2}{EE_{ij}} \ln E + O(E^{-2}, E^{-3}, \ldots), \qquad (9)$$

where a_o is the Bohr radius, R is the Rydberg energy, E_{ij} is the excitation energy from the initial to final level, and f_{ij} is the optical oscillator strength of the $i \rightarrow j$ transition. The $E^{-1} \ln E$ relation in the first term is associated with the characteristic broad maximum observed in the energy dependence of the excitation cross sections corresponding to dipole-allowed transitions. However, when f_{ij} is small the higher-order terms become more prominent resulting in a change in the excitation function toward a narrower peak that reflects the E^{-n} components. Such a bridging is indeed evident in our data. Of the four dipole-allowed excitations reported here, the $1s_5 \rightarrow 3p_8$ and $1s_5 \rightarrow 3p_6$ have the largest oscillator strengths (0.0114 and 0.0075, respectively), and their excitation functions are clearly characterized by a broad maximum, albeit with a small structure near threshold for $1s_5 \rightarrow 3p_6$.

Continuing onto the third graph ($1s_5 \rightarrow 3p_9$) of Fig. 4 where the optical oscillator strength f_{ij} is reduced to 0.0025, the cross section between 5–10 eV remains rather flat like the

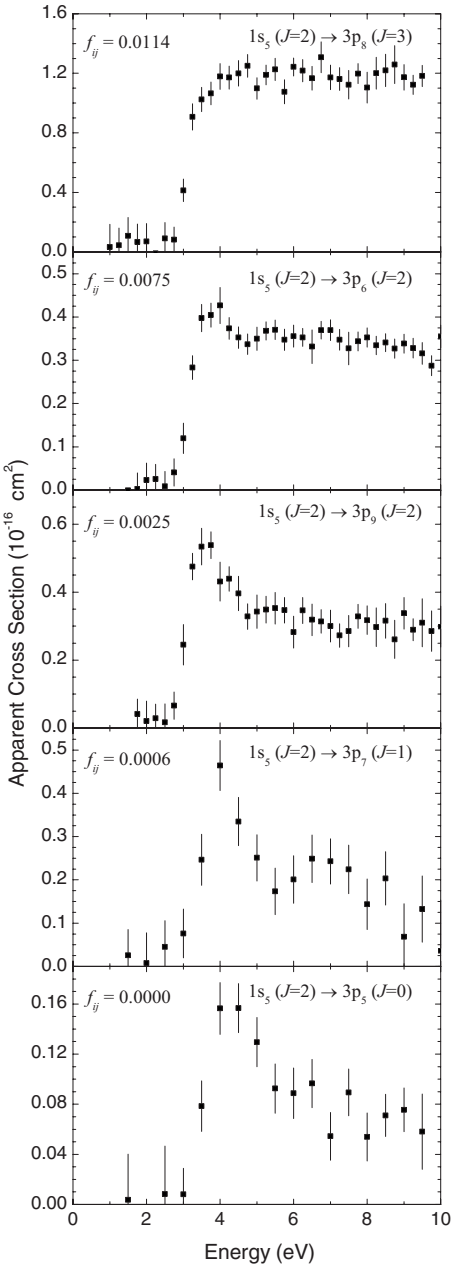

FIG. 4. Apparent cross sections for electron excitation from the $1s_5(J=2)$ metastable level into levels of the Xe($5p^5 7p$) configuration. Error bars are statistical only and do not include the uncertainty in the absolute calibration (±40%) and transition probabilities used to convert Q^{opt} to Q^{app}.

two graphs above it. On the other hand, the near-threshold structure which is barely discernable in the second graph ($1s_5 \rightarrow 3p_6$), now develops into a full-fledged peak echoing the earlier suggestion of a stronger presence of the higher-order terms when f_{ij} becomes small. The $1s_5 \rightarrow 3p_7$ excitation function (fourth graph) corresponds to the smallest f_{ij} of 0.0006, and a cursory inspection of the cross-section curve does indicate an even more prominent near-threshold structure around 4 eV. However, the error bars in the $1s_5 \rightarrow 3p_7$ data are substantially larger than the case of $1s_5 \rightarrow 3p_9$, thus one must be careful in comparing the shape of the excitation function. As a quantitative measure of the prominence of the near-threshold structure, we examine the ratios of the cross sections at 4, 4.5, and 5 eV, i.e., $Q(4.5\ \mathrm{eV})/Q(4\ \mathrm{eV})$ and $Q(5\ \mathrm{eV})/Q(4\ \mathrm{eV})$. For the $1s_5 \rightarrow 3p_9$ excitation where the error bars are relatively small, we calculate these ratios using the data points (■) in the graph which give $Q(4.5\ \mathrm{eV})/Q(4\ \mathrm{eV})=0.92$ and $Q(5\ \mathrm{eV})/Q(4\ \mathrm{eV})=0.79$. Turning to $1s_5 \rightarrow 3p_7$, where the error bars are much larger we get $Q(4.5\ \mathrm{eV})/Q(4\ \mathrm{eV})=0.72$ and $Q(5\ \mathrm{eV})/Q(4\ \mathrm{eV})=0.54$ if we use the data points in the graph, indicating a much steeper decent of the excitation function. However we need to address the uncertainty introduced by the larger error bars. For this purpose we consider the worst extreme scenario where we take the lowest limit of the cross section (given by the error bar) at 4 eV, but use the upper limit for cross sections at 4.5 and 5 eV in order to suppress as much as possible the visibility of the near-threshold feature. The ratios now become $Q(4.5\ \mathrm{eV})/Q(4\ \mathrm{eV})=0.96$ and $Q(5\ \mathrm{eV})/Q(4\ \mathrm{eV})=0.75$. Considering that this worst extreme situation is extremely unlikely, we see that the $1s_5 \rightarrow 3p_7$ excitation shows even more departure from the standard dipole-allowed prototype as compared to $1s_5 \rightarrow 3p_9$. Finally the $1s_5 \rightarrow 3p_5$ excitation is a dipole-forbidden case and the cross-section data are indeed completely devoid of the broad maximum feature.

Although the magnitudes of the cross sections (at 8 eV) for all five cases are qualitatively in the order of their respective oscillator strengths, no simple quantitative correlation is apparent. This is in contrast to our findings for Ar($1s_5 \rightarrow 2p_x$) and Xe($1s_5 \rightarrow 2p_x$) excitations where the cross section scales with the oscillator strength [7,9]. This scaling relation is not only interesting but also has a practical utility since it allows us to estimate cross sections where experimental data are not available. The absence of such a scaling rule for Xe($1s_5 \rightarrow 3p_x$) is naturally disappointing. Nevertheless, a similar unfortunate situation also exists in Ar($1s_5 \rightarrow 3p_x$) where the cross sections do not track well with the oscillator strengths [10].

To understand the physical origin of the variance between the $1s_5 \rightarrow 2p_x$ and $1s_5 \rightarrow 3p_x$ series reported above, some clarifying remarks concerning our usage of the Born-Bethe theory to analyze the experimental data are in order. In reference to the Born-Bethe expansion as given in Eq. (9) it is customary to make a further approximation of retaining only the leading term

$$Q_{ij}^{BB}(E) \simeq 4\pi a_o^2 f_{ij} \frac{R^2}{E E_{ij}} \ln E, \tag{10}$$

reflecting the well-known connection of cross section with oscillator strength and the $E^{-1}\ln E$ energy dependence. Application of this equation to our data, however, must be made with care since it is valid only at high energies. For instance, Eq. (10) does not reproduce quantitatively the shape of the observed excitation function near the maximum; only at energies well above the peak region does Eq. (10) make a reasonable approximation. Nevertheless, we can speak of a broad or narrow peak in a qualitative way depending on whether the cross sections vary like $E^{-1}\ln E$ or $E^{-n}(n \geq 1)$ at high energies. Looking at the general shape of the curves in Fig. 4 we should not expect Eq. (10) to be valid at 8 eV

TABLE IV. Optical emission cross sections for excitation out of the $1s_5(J=2)$ metastable level at 8 eV. Entries for dipole-forbidden transitions are left blank. Values obtained via branching fractions are indicated in parenthesis. Uncertainties in total apparent cross sections (Q^{App}) include statistical and systematic uncertainties from measured emission cross sections and the additional uncertainties introduced by using branching fractions from Ref. [12] to fill in unmeasured transitions.

	Cross Section (10^{-16} cm^2)				
Lower level	$3p_5(J=0)$	$3p_6(J=2)$	$3p_7(J=1)$	$3p_8(J=3)$	$3p_9(J=2)$
$1s_2(J=1)$	(0.019)	(0.042)	(0.035)		(0.028)
$1s_3(J=0)$			(0.049)		
$1s_4(J=1)$	0.016	(0.025)	0.008		0.041
$1s_5(J=2)$		0.092	(0.0004)	0.341	(0.031)
$\Sigma 5p^5 7s$	(0.010)	(0.124)	(0.025)	(0.51)	(0.104)
$\Sigma 5p^5 5d$	(0.008)	(0.070)	(0.027)	(0.25)	(0.114)
Q^{App}	(0.053 ± 0.030)	(0.353 ± 0.140)	(0.144 ± 0.060)	(1.10 ± 0.45)	(0.318 ± 0.130)

which is still in the neighborhood of the peak. Thus our observation of the excitation cross section not being proportional to the oscillator strength in the Ar($1s_5 \rightarrow 3p_x$) and Xe($1s_5 \rightarrow 3p_x$) series is not a surprise. What is really surprising is the Xe($1s_5 \rightarrow 2p_x$) excitation series, and also Ar($1s_5 \rightarrow 2p_x$), where the cross section for excitation into a particular final state ($2p_x$) within the series remains approximately proportional to the corresponding oscillator strength even at energies almost down to the excitation threshold.

To view this situation from a more quantitative perspective, we express the $i \rightarrow j$ electron excitation cross section, $Q_{ij}(E)$ (units of πa_0^2) as

$$Q_{ij}(E) = \frac{1}{E}\frac{8}{\Delta E_{ij}}\int_{K_{\min}}^{K_{\max}} f_{ij}(K)d(\ln K), \tag{11}$$

where E is the incident electron energy (in Rydbergs), ΔE_{ij} is the excitation threshold, K is the momentum transferred (divided by $\hbar$), and $f_{ij}(K)$ is the generalized oscillator strength. The limits of integration, $K_{\min}$ and $K_{\max}$, which are functions of ΔE_{ij} and E, correspond to forward and backward scattering. Values for the generalized oscillator strengths for Xe($1s_5 \rightarrow 2p_x$) and Xe($1s_5 \rightarrow 3p_x$) excitation processes were calculated using the method of Ref. [26].

A plot of the generalized oscillator strength $f_{ij}(K)$ against K shows a constant value from $K=0$ through $K \sim 0.1a_o^{-1}$ followed by a monotonic decline at higher K as illustrated in the upper block of Fig. 5 for the case of Xe($1s_5 \rightarrow 2p_8$). The $f_{ij}(K)$ curves for the other $1s_5 \rightarrow 2p_x$ members have the same shape and differ only in the asymptotic value $f_{ij}(K=0)$. Since the observed excitation cross section corresponds to the area under this curve between $K_{\min}$ and $K_{\max}$, the excitation cross sections for different members of the $1s_5 \rightarrow 2p_x$ series at a given energy vary according to the respective $f_{ij}(K=0)$ which is the optical oscillator strength. The shape of the $f_{ij}(K)$ curve, however, is very different for the $1s_5 \rightarrow 3p_x$ series. For instance, $f_{ij}(K)$ for $1s_5 \rightarrow 3p_8$ excitation starts with a constant value from $K=0$ to $K \sim 0.1a_o^{-1}$ then rises to a maximum value almost three times $f_{ij}(K=0)$, as shown in the lower block of Fig. 5. At low electron energies the range of the K parameter is such that the excitation cross section corresponds only to the area of the $f_{ij}(K)$ curve near the peak, bearing little apparent relation to the optical oscillator strength. Unlike the case for $1s_5 \rightarrow 2p_x$ excitation where the generalized oscillator curve is characterized by the single scaling parameter $f_{ij}(K=0)$, the $1s_5 \rightarrow 3p_x$ curve has two effective parameters, $f_{ij}(K=0)$ and $f_{ij}(K \approx 0.3a_o^{-1})$. To the ex-

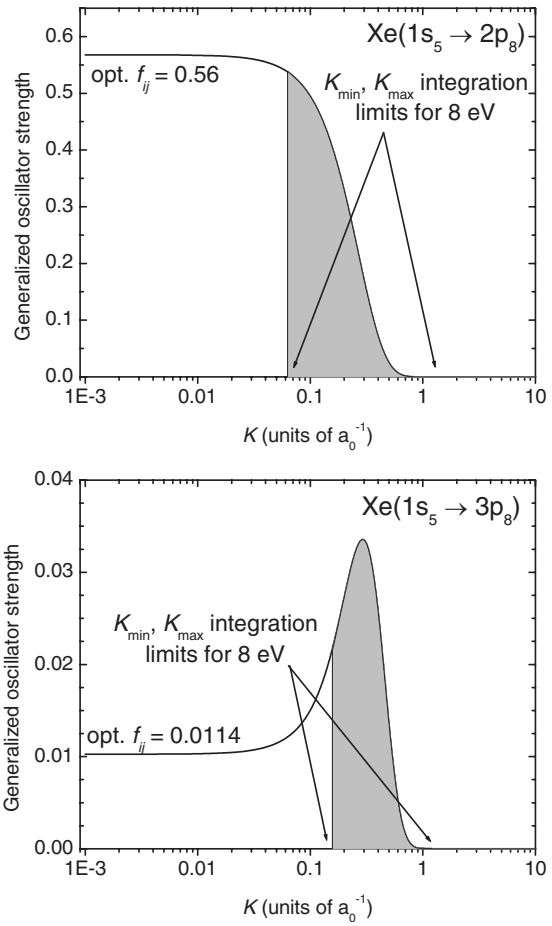

FIG. 5. Generalized oscillator strengths for the ($J=2 \rightarrow J=3$) Xe($1s_5 \rightarrow 2p_8$) and Xe($1s_5 \rightarrow 3p_8$) excitation processes.

tent that these are independent of one another, the $1s_5 \rightarrow 3p_x$ excitation cross sections at low energies will in general be independent of the f_{ij} scaling. The variations of the generalized oscillator strength with respect to K for both Xe($1s_5 \rightarrow 2p_8$) and Xe($1s_5 \rightarrow 3p_8$) indeed closely parallel to what we have seen in Ar [10].

Before leaving this section we must emphasize that the close tracking of the $1s_5 \rightarrow 2p_x$ excitation cross sections near the threshold region is not to be taken as a validation of Eq. (10) at low energies. Clearly the energy dependence of all our $1s_5 \rightarrow 2p_x$ cross section data in the 2–10 eV region does not conform to the $E^{-1} \ln E$ expression. The observed relation between excitation cross section and oscillator strength for the $1s_5 \rightarrow 2p_x$ series is not a consequence of Eq. (10), but rather stems from the particular shape of the $f_{ij}(K)$ curve.

E. Comparison to other work

The *optical emission cross section* for excitation from the $1s_5(J=2)$ into the $3p_8(J=3)$ level using the $3p_8 \rightarrow 1s_5$ (467.1 nm) emission line has been previously measured by Mityureva and Smirnov [27], using a two-pulse electron-beam method [28]. In their technique, a high-energy pulse first excites atoms into the metastable level from the ground state, and a second low-energy pulse excites atoms into $5p^57p$ levels. They report a peak optical emission cross-section value of 2.2×10^{-16} cm^2 ($\pm 50\%$) at an electron energy of 6 eV and falling to a value of 1.1×10^{-16} cm^2 ($\pm 30\%$) at 8 eV. This seemingly peaky shape is in sharp contrast to the present results as well as all previous works in rare gases in which a broad peak is found for excitation from $1s_5$ into the $J=3$ level of the $2p$ and $3p$ groups. In addition, the overall magnitude at 8 eV appears to be nearly a factor of 3 larger than the value obtained in this work.

Examination of cross-section data for excitation out of the metastable levels of Kr and Xe provides further insight to the physics of the excitation process. For the heavy rare gases (Kr and Xe) three major parameters to consider when comparing cross sections are (i) the energy difference (ΔE) between the initial and final levels involved in the excitation process, (ii) whether or not the excitation process is dipole allowed according to the familiar selection rules (i.e., $\Delta J = 0, \pm 1$; with $J=0 \not\rightarrow J=0$), and (iii) whether or not the core angular-momentum quantum number j_c of the initial and final levels is preserved in the excitation process. The significance of this latter parameter was made apparent through our prior work on Kr [29] and Xe [7]. As an interesting case, we compare the present results for excitation from the $1s_5$ metastable level into the six $5p^57p$ levels corresponding to the core angular momentum $j_c=3/2$ with previously measured cross sections for excitation into the four $5p^56p$ levels corresponding to $j_c=1/2$ (called $5p^56p'$). Note that these two groups have similar excitation energies (ΔE) as depicted in Fig. 1, and can be used to expose the relative importance of parameters (ii) and (iii). Observations from prior work on all of the rare gases demonstrate that cross sections corresponding to dipole-allowed processes are in general larger than dipole-forbidden processes and that cross sections corresponding to core preserving processes (especially in the heavy rare gases Kr and Xe) have been shown to be larger than those changing the core [4]. Furthermore, based on experiments in Ar, cross sections for excitation out of the $1s_5$ metastable level into the $2p$ manifold are on average an order of magnitude or more larger than cross sections into the $3p$ manifold [10]. In light of these trends we discuss a specific comparison of the Xe($1s_5 \rightarrow 3p_5$) cross section measured in this work to the Xe($1s_5 \rightarrow 2p_4$) cross section previously measured [7]. In this comparison, the $1s_5 \rightarrow 3p_5$ excitation process is dipole forbidden ($J=2 \rightarrow J=0$) but core preserving ($j_c=3/2 \rightarrow j_c=3/2$), while the $1s_5 \rightarrow 2p_4$ excitation is dipole allowed ($J=2 \rightarrow J=2$) but core changing ($j_c=3/2 \rightarrow j_c=1/2$). Furthermore, having $\Delta n=2$ places the $1s_5 \rightarrow 3p_5$ process at a distinct disadvantage to the more favorable $\Delta n=1$ $1s_5 \rightarrow 2p_4$ process. We estimated the $1s_5 \rightarrow 2p_4$ cross section to be much less than 0.2×10^{-16} cm^2 [7], which is *at most* on par with the $1s_5 \rightarrow 3p_5$ cross section (the smallest of those measured in this work). The results of this comparison suggest that the excitation process favors core preservation over the dipole-type coupling. This is in agreement with previous experiments on Kr [29].

IV. CONCLUDING REMARKS

In low-temperature plasmas, Xe($5p^57p$) levels are populated via electron-impact excitation from both the ground state as well as the metastable level(s). In this regard, it is enlightening to examine two ways in which the metastable cross sections from Sec. III differ from the ground-state cross sections measured in Sec. II. First, the peak cross section into a given Xe($3p_x$) level out of the $1s_5$ metastable level is 12 to 51 times the peak cross section out of the ground state. Second the threshold energy (ΔE_{ij}) into the Xe($3p_x$) levels out of the metastable levels is considerably smaller ($\sim$2.7 eV) than that out of the ground state ($\sim$11 eV). While the metastable cross sections are, on average, only an order of magnitude larger than their ground-state counterparts, the much lower excitation thresholds ensure that in a low-temperature plasma, which contains far more low-energy electrons than high-energy electrons, excitation from the metastable levels may be significant. Indeed, in the case of emissions from the Xe($2p_x$) levels, for which the cross sections out of the metastable levels ($\sim$1.5 eV threshold) range from 8.3 to 200 times the ground-state values ($\sim$9.8 eV threshold), Donnelly and Schabel suggested that in their experiment on inductively coupled plasmas, metastables account for 76% or more of the excitation into levels having large Q_m/Q_g ratios (i.e., Xe($2p_8$) having $Q_m/Q_g=200$), whereas for other levels (i.e., Xe($2p_5$) having $Q_m/Q_g=8.3$) the excitation from the ground state accounts for $>80\%$ [30].

It is interesting to note that the difference between excitation out of the metastable level and ground state is generally smaller for the Xe($3p_x$) levels than the Xe($2p_x$) levels. Similar variations between the metastable and ground-state cross sections have also been observed in Ar where the ratios for excitation into the Ar($2p_x$) and Ar($3p_x$) levels range from 27–500 and 11–56, respectively [9,10]. In this context, the peak metastable to ground-state cross sections are generally largest for excitation into Ar($2p_x$) levels followed by Xe($2p_x$)

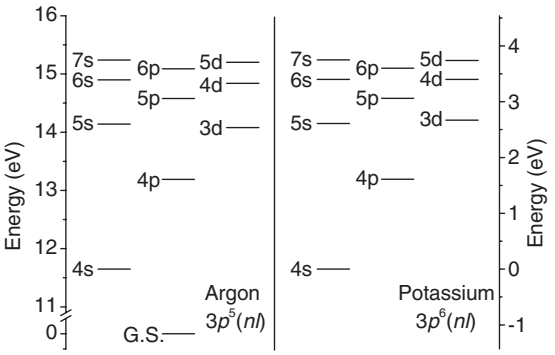

FIG. 6. Energy levels of argon and potassium shown for relative comparison.

and then by Ar($3p_x$) and Xe($3p_x$). This ordering correlates well with the ratios of excitation thresholds out of ground and metastable levels. This is largest for the Ar($2p_x$) levels (13.2 eV/1.6 eV≈8.3), decreases some for the Xe($2p_x$) levels (≈6.5), and is much smaller for the Ar($3p_x$) and Xe($3p_x$) levels (4.8 and 4.1, respectively).

For the purposes of optical plasma diagnostics and modeling Xe plasma light emissions, it is sometimes more useful to work with optical emission cross sections rather than the apparent excitation cross sections reported in this paper. These values can be easily computed from the apparent cross sections from the ground and metastable levels given in Figs. 2 and 4 by multiplying by the appropriate branching fractions from Table I, i.e., Eq. (6).

ACKNOWLEDGMENT

Support by the National Science Foundation is gratefully acknowledged.

APPENDIX

We present our model calculations of the cascade contributions to excitation out of the metastable levels into the $3p^54p$ and $3p^55p$ levels of Ar and into the $5p^56p$ and $5p^57p$ levels of Xe. An interesting result of this model analysis is the strong contrast between the results of Ar and Xe which can be traced to the electronic structure of the atoms. Consider first cascade into Ar($3p^54p$). Here we are concerned with cascades from the $3p^53d$, $3p^54d$, $3p^55d$, $3p^55s$, $3p^56s$, and $3p^57s$ levels. To find the cascades, we need (i) the cross sections for excitation from the metastable levels ($3p^54s$) into the $3p^5nd$ and $3p^5ns$ series and (ii) the branching fractions of the relevant $3p^5nd \rightarrow 3p^54p$ and $3p^5ns \rightarrow 3p^54p$ arrays. Values for part (ii) are available in the literature [31,32]. To estimate the unknown cross sections in part (i), we note the close correspondence between the $n'p^5nl$ levels of the rare gases ($n'=2,3,4,5$ for Ne, Ar, Kr, Xe) and the $n'p^6nl$ levels of the alkalis. If we compare the centroid of the levels of the $n'p^5nl$ configuration of the rare-gas with the corresponding alkali $n'p^6nl$ levels, we find practically the same level spacings for the two sets. This is shown in Fig. 6 for the case of Ar($3p^5nl$) vs K($3p^6nl$); the same kind of similarity is also found for Ne vs Na, Kr vs Rb, and Xe vs Cs. In our model we treat the levels from each Ar($4p^5nl$) configuration as a single aggregate and assume that the Ar($3p^54s \rightarrow 3p^5nl$) excitation cross sections are related to the corresponding K($3p^64s \rightarrow 3p^6nl$) cross sections by a scaling factor. Since the percentage cascade from Ar($3p^5nl$) into Ar($3p^54p$) depends only on the ratio of Ar($3p^54s \rightarrow 3p^5nl$) to Ar($3p^54s \rightarrow 3p^54p$) excitation cross sections, we use the measured apparent excitation cross sections of K($3p^64s \rightarrow 3p^6nl$) [33] at 10 eV to obtain the Ar cross-section ratios needed for cascade analysis. In order to handle the individual levels from a configuration as a single manifold, we sum the individual transition probabilities of the $3p^5nl \rightarrow 3p^54p$ arrays over the lower level and average over the upper level to obtain an effective transition probability for the $3p^5nl \rightarrow 3p^54p$ cascade. Applying this procedure to examine the cascades into Ar($3p^54p$) from the $3p^55s$, $3p^56s$, $3p^57s$, $3p^53d$, $3p^54d$, and $3p^55d$, we find that 17% of the apparent cross section is due to cascade from the higher levels and more than four-fifths of the total cascade came from the $3p^53d$ configuration. The fractional cascade component for excitation into Ar($3p^54p$) from the metastable level has been measured by a time-resolution-like experiment with the result of ~10% [9,34].

Consider next, excitation of metastable levels of argon to the Ar($3p^55p$) levels. We perform the same model calculation for the cascades from $3p^56s$, $3p^57s$, $3p^54d$, and $3p^55d$, and estimate the cascade to be 27% of the apparent excitation cross section. Again, more than four-fifths of the total cascade is from just one configuration which is $3p^54d$ in this case.

For excitation from the metastable level of Xe into the Xe($5p^5nl$) groups, the alkali counterparts are Cs($6S \rightarrow nL$). Unfortunately most of the Cs excitation cross sections needed are not known. To estimate the Cs cross sections we assume a scaling relation between the Rb($5S \rightarrow nL$) excitation cross sections and the corresponding Cs[$6S \rightarrow (n+1)L$] analog. Using a set of Rb excitation cross sections derived from experimental measurements [35,36] and theoretical calculations [37], we obtain the relevant Xe cross-section ratios for calculating cascades from the Xe($5p^57s$), Xe($5p^58s$), Xe($5p^59s$), Xe($5p^55d$), Xe($5p^56d$), and Xe($5p^57d$) levels into Xe($5p^56p$). Transition probabilities given in Ref. [38] are used to calculate the effective branching fractions. Our model calculation gives the cascade component as 21% of the Xe($5p^56p$) apparent excitation cross section, with the $5p^55d$ alone accounting for four-fifths of the total cascade.

Finally we come to consider the cascade component of the Xe($5p^57p$) apparent cross sections. In all three preceding cases, by far the largest source of cascade into a given Ar($2p$), Ar($3p$), or Xe($2p$) configuration arises from the $n'd$ configuration immediately above it. Thus we would expect the Xe($5p^57p$) levels to receive cascade mostly from Xe($5p^56d$). Interestingly this turns out not to be the case. The "anomaly" occurs because the Xe($5p^56d$) manifold is only very slightly (0.07 eV) above Xe($5p^57p$) resulting in exceptionally small $5p^56d \rightarrow 5p^57p$ emission probabilities with an effective branching fraction of 0.0008. This virtually eliminates the $5p^56d \rightarrow 5p^57p$ cascade channel even though the $5p^56d$ levels themselves could be significantly populated by electron excitation of the metastables. The fractional cascade to Xe($5p^57p$) is now found to be ~5%.

Even with a significant uncertainty in our estimates of the cross-section ratios, we can always expect that because of the very small energy difference between $5p^5 6d$ and $5p^5 7p$, the major source of cascade (i.e., typically the next higher "*d*" configuration) into $5p^5 7p$ is eliminated resulting in an unusually small cascade component of the apparent excitation cross section. Nevertheless in view of the approximate nature of the model, we place our estimate of fractional cascade as being less than 10%.

Qualitatively, the small $5p^5 6d \rightarrow 5p^5 7p$ transition probabilities will also limit the cascade contribution of the $5p^5 6d$ levels for excitation *from the ground state*. However, we cannot provide a quantitative estimate owing to a lack of a surrogate set of cross sections out of the ground state equivalent to the metastable/alkali combination used in the above model. It should also be noted that the typical cascade contribution is on the order of the listed percentage and that the percentage is not an *average*. Furthermore, the percentage of cascades into levels having a small direct excitation cross section could be larger than the percentage of cascades into levels having large direct cross sections.

[1] D. Uhrlandt, R. Bussiahn, S. Gorchakov, H. Lange, D. Loffhagen, and D. Nötzold, J. Phys. D **38**, 3318 (2005).
[2] Y. Chiu, B. L. Austin, S. Williams, R. A. Dressler, and G. F. Karabadzhak, J. Appl. Phys. **99**, 113304 (2006).
[3] G. F. Karabadzhak, Y. Chiu, and R. A. Dressler, J. Appl. Phys. **99**, 113305 (2006).
[4] J. B. Boffard, R. O. Jung, L. W. Anderson, and C. C. Lin, Adv. At., Mol., Opt. Phys. **54**, 319 (2006).
[5] J. T. Fons and C. C. Lin, Phys. Rev. A **58**, 4603 (1998).
[6] R. O. Jung, T. E. Stone, J. B. Boffard, L. W. Anderson, and C. C. Lin, Phys. Rev. A **73**, 022722 (2006).
[7] R. O. Jung, J. B. Boffard, L. W. Anderson, and C. C. Lin, Phys. Rev. A **72**, 022723 (2005).
[8] V. M. Donnelly, J. Phys. D **37**, R217 (2004).
[9] J. B. Boffard, G. A. Piech, M. F. Gehrke, L. W. Anderson, and C. C. Lin, Phys. Rev. A **59**, 2749 (1999).
[10] R. O. Jung, J. B. Boffard, L. W. Anderson, and C. C. Lin, Phys. Rev. A **75**, 052707 (2007).
[11] E. B. Saloman, J. Phys. Chem. Ref. Data **33**, 765 (2004).
[12] R. O. Jung, J. B. Boffard, L. W. Anderson, and C. C. Lin, J. Quant. Spectrosc. Radiat. Transf. **110**, 1057 (2009).
[13] A. R. Filippelli, C. C. Lin, L. W. Anderson, and J. W. McConkey, Adv. At., Mol., Opt. Phys. **33**, 1 (1994).
[14] A. R. Filippelli, S. Chung, and C. C. Lin, Phys. Rev. A **29**, 1709 (1984).
[15] B. Van Zyl, G. H. Dunn, G. Chamberlain, and D. W. O. Heddle, Phys. Rev. A **22**, 1916 (1980).
[16] K. G. Walker (private communication).
[17] Y. M. Smirnov, Opt. Spectrosc. **92**, 357 (2002).
[18] P. V. Fel'tsan and I. P. Zapesochnyi, Ukr. Phys. J. **13**, 143 (1968).
[19] G. S. Rostovikova, V. P. Samoilov, and Y. M. Smirnov, Opt. Spectrosc. **34**, 3 (1973).
[20] H. Horiguchi, R. S. F. Chang, and D. W. Setser, J. Chem. Phys. **75**, 1207 (1981).
[21] K.-P. Nick and V. Helbig, Phys. Scr. **32**, 111 (1985).
[22] D. R. Bates and A. Damgaard, Philos. Trans. R. Soc. London, Ser. A **242**, 101 (1949).
[23] J. E. Chilton, M. D. Stewart, Jr., and C. C. Lin, Phys. Rev. A **61**, 052708 (2000).
[24] J. E. Chilton, J. B. Boffard, R. S. Schappe, and C. C. Lin, Phys. Rev. A **57**, 267 (1998).
[25] J. E. Chilton, M. D. Stewart, Jr., and C. C. Lin, Phys. Rev. A **62**, 032714 (2000).
[26] R. D. Cowan, *The Theory of Atomic Structure and Spectra* (University of California Press, Berkeley, 1981).
[27] A. A. Mityureva and V. V. Smirnov, Opt. Spectrosc. **75**, 417 (1993).
[28] A. A. Mityureva and V. V. Smirnov, Opt. Spectrosc. **74**, 6 (1993).
[29] R. O. Jung, T. E. Stone, J. B. Boffard, L. W. Anderson, and C. C. Lin, Phys. Rev. Lett. **94**, 163202 (2005).
[30] V. M. Donnelly and M. J. Schabel, J. Appl. Phys. **91**, 6288 (2002).
[31] National Institute of Standards and Technology, http://physics.nist.gov/PhysRefData/ASD/.
[32] O. Zatsarinny and K. Bartschat, J. Phys. B **39**, 2145 (2006).
[33] J. O. Phelps, J. E. Solomon, D. F. Korff, C. C. Lin, and E. T. P. Lee, Phys. Rev. A **20**, 1418 (1979).
[34] J. B. Boffard, M. F. Gehrke, M. E. Lagus, L. W. Anderson, and C. C. Lin, Eur. Phys. J. D **8**, 193 (2000).
[35] Z. Wei, C. Flynn, A. Redd, and B. Stumpf, Phys. Rev. A **47**, 1918 (1993).
[36] S. T. Chen and A. C. Gallagher, Phys. Rev. A **17**, 551 (1978).
[37] T. J. Greene and W. Williamson, Jr., At. Data Nucl. Data Tables **14**, 161 (1974).
[38] M. Aymar and M. Coulombe, At. Data Nucl. Data Tables **21**, 537 (1978).